Monotonic quantum-to-classical transition enabled by positively correlated biphotons

Rui-Bo Jin,[1,*] Guo-Qun Chen,[1] Hui Jing,[2] Changliang Ren,[3] Pei Zhao,[1] Ryosuke Shimizu,[4,†] and Pei-Xiang Lu[1,‡]

[1]*Laboratory of Optical Information Technology and School of Material Science and Engineering, Wuhan Institute of Technology, Wuhan 430205, China*

[2]*Key Laboratory of Low-Dimensional Quantum Structures and Quantum Control of Ministry of Education, Department of Physics and Synergetic Innovation Center for Quantum Effects and Applications, Hunan Normal University, Changsha 410081, China*

[3]*Chongqing Institute of Green and Intelligent Technology, Chinese Academy of Sciences, Chongqing 400714, China*

[4]*University of Electro-Communications, 1-5-1 Chofugaoka, Chofu, Tokyo 182-8585, Japan*

(Received 15 April 2017; published 29 June 2017)

Multiparticle interference is a fundamental phenomenon in the study of quantum mechanics. It was discovered in a recent experiment [Y.-S. Ra *et al.*, Proc. Natl. Acad. Sci. USA **110**, 1227 (2013)] that spectrally uncorrelated biphotons exhibited a nonmonotonic quantum-to-classical transition in a four-photon Hong-Ou-Mandel (HOM) interference. In this work, we consider the same scheme with spectrally correlated photons. By theoretical calculation and numerical simulation, we found the transition not only can be nonmonotonic with negatively correlated or uncorrelated biphotons, but also can be monotonic with positively correlated biphotons. The fundamental reason for this difference is that the HOM-type multiphoton interference is a differential-frequency interference. Our study may shed new light on understanding the role of frequency entanglement in multiphoton behavior.

DOI: 10.1103/PhysRevA.95.062341

I. INTRODUCTION

Indistinguishability plays an important role in multiphoton interference, which is a fundamental phenomenon in the study of quantum mechanics [1–6]. It was believed that, with the increase of indistinguishability, the multiphoton interference pattern changes monotonically [1]. For example, in the case of Hong-Ou-Mandel (HOM) interference demonstrated in 1987 [7], the twofold coincidence counts show a monotonic increase when the time delay scanned from zero to infinity. This HOM interference can be interpreted from the viewpoint of indistinguishability: with the increase of the time delay, the temporal distinguishability (or the decoherence) of the biphoton was also increasing and leading to a quantum-to-classical transition [1,8,9]. Such a monotonic indistinguishability dependence was also observed in the case of four-photon [10] and six-photon [11] HOM-type interference, where all photons are detected in one output port of the beam splitter.

However, recent works [1,12,13] revealed that such monotonic quantum-to-classical transition was only an exception, i.e., only valid for two-photon cases and for bunching detection in multiphoton cases. For example, in the four-photon HOM-type experiment [1], where two pairs of biphotons were sent to two input ports of a 50:50 beam splitter and four detectors were prepared at the two output ports (see Fig. 1), by changing the detection schemes, different interference patterns can be obtained: in a $2/2$ detection [with two detectors at one output port and two detectors at the other port, shown in Fig. 1(a)], the fourfold coincidence counts showed a nonmonotonic indistinguishability dependence; in contrast, the $4/0$ detection scheme, as shown in Fig. 1(c), achieved a monotonic dependence. This study on the transition between quantum and classical in Ref. [1] is important for deeper understanding of the multiparticle behavior in quantum mechanics.

The interesting phenomenon in Ref. [1] was realized by spectrally uncorrelated biphotons. Now a question comes naturally: what will the phenomenon be if the biphotons are spectrally correlated? In other words, with the introduction of frequency entanglement, will the interference patterns, especially the monotonicity dependence, be changed? To answer this question, in this paper, we consider the same scheme with spectrally correlated (frequency-entangled) biphotons. It is seen that spectrally correlated biphotons show different interference patterns from the patterns of uncorrelated biphotons. For example, under the $2/2$ detection scheme, the spectrally negatively correlated and noncorrelated biphotons show a nonmonotonic dependence, while the spectrally positively correlated biphotons show a monotonic dependence. In contrast, the monotonicity is not affected by the spectral correlation in the $4/0$ and $3/1$ detection schemes.

This paper is organized as follow: in the Introduction section, we provide the background and motivation of this research. Then, in the Theory section we develop a multimode theory for four-photon HOM-type interference, where the spectral correlation between the signal and idler photons are concerned. Next, in the Analysis section, we first simulate the HOM-type interference patterns using biphotons with three different spectral correlations: no correlation, positive correlation, and negative correlation. Then, we provide comprehensive discussions on the simulation results. Finally, we summarize the paper in the Conclusion section. More details for the derivation of the relative equations are given in the Appendix.

II. THEORY

In this paper, we consider a four-photon HOM-type interference with the experimental model shown in Fig. 1.

*jrbqyj@gmail.com
†r-simizu@pc.uec.ac.jp
‡lupeixiang@hust.edu.cn

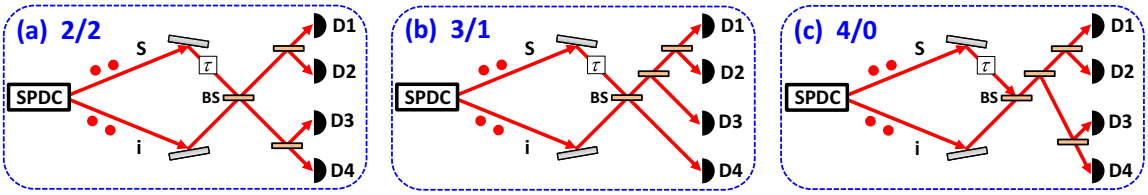

FIG. 1. The 2/2, 3/1, and 4/0 detection schemes for the HOM-type interference. All the beam splitters (BS) are 50:50 beam splitters. D_n ($n = 1,2,3,4$) is the single photon detector. τ is the time delay in the signal arm.

The four-photon state $|\psi\rangle$ is generated from the two-pair components in a spontaneous parametric down-conversion (SPDC) process,

$$|\psi\rangle = \int_0^\infty d\omega_s d\omega_i d\omega_s' d\omega_i' f(\omega_s,\omega_i) f(\omega_s',\omega_i') \times \hat{a}_s^\dagger(\omega_s)\hat{a}_i^\dagger(\omega_i)\hat{a}_s^\dagger(\omega_s')\hat{a}_i^\dagger(\omega_i')|0000\rangle, \quad (1)$$

where $\hat{a}^\dagger(\omega)$ is the creation operator at angular frequency ω, the subscripts s and i denote the signal and idler photons from the first pair, while s' and i' denote the signal and idler photons from the second pair; $f(\omega_s,\omega_i)$ and $f(\omega_s',\omega_i')$ are their joint spectral amplitude (JSA).

As calculated in detail in the Appendix, the fourfold coincidence probability $P_{22}(\tau)$ in the 2/2 detection scheme is

$$P_{22}(\tau) = \frac{1}{64}\int_0^\infty d\omega_1 d\omega_2 d\omega_3 d\omega_4 |I_{22}(\tau)|^2, \quad (2)$$

with

$$\begin{aligned}|I_{22}(\tau)|^2 = |&(f_{13}f_{24} + f_{14}f_{23})e^{-i\omega_1\tau}e^{-i\omega_2\tau} \\ &+ (f_{31}f_{42} + f_{32}f_{41})e^{-i\omega_3\tau}e^{-i\omega_4\tau} \\ &- (f_{12}f_{34} + f_{14}f_{32})e^{-i\omega_1\tau}e^{-i\omega_3\tau} \\ &- (f_{12}f_{43} + f_{13}f_{42})e^{-i\omega_1\tau}e^{-i\omega_4\tau} \\ &- (f_{21}f_{34} + f_{24}f_{31})e^{-i\omega_2\tau}e^{-i\omega_3\tau} \\ &- (f_{21}f_{43} + f_{23}f_{41})e^{-i\omega_2\tau}e^{-i\omega_4\tau}|^2, \end{aligned} \quad (3)$$

where $f_{mn} = f(\omega_m,\omega_n)$ and $\omega_{m(n)}$ $[m(n) = 1,2,3,4]$ is the frequency of the detection field for the detectors D_n.

The coincidence probability $P_{31}(\tau)$ in the 3/1 detection scheme is

$$P_{31}(\tau) = \frac{1}{128}\int_0^\infty d\omega_1 d\omega_2 d\omega_3 d\omega_4 |I_{31}(\tau)|^2, \quad (4)$$

with

$$\begin{aligned}|I_{31}(\tau)|^2 = |&-(f_{13}f_{24} + f_{14}f_{23})e^{-i\omega_1\tau}e^{-i\omega_2\tau} \\ &+ (f_{31}f_{42} + f_{32}f_{41})e^{-i\omega_3\tau}e^{-i\omega_4\tau} \\ &- (f_{12}f_{34} + f_{14}f_{32})e^{-i\omega_1\tau}e^{-i\omega_3\tau} \\ &+ (f_{12}f_{43} + f_{13}f_{42})e^{-i\omega_1\tau}e^{-i\omega_4\tau} \\ &- (f_{21}f_{34} + f_{24}f_{31})e^{-i\omega_2\tau}e^{-i\omega_3\tau} \\ &+ (f_{21}f_{43} + f_{23}f_{41})e^{-i\omega_2\tau}e^{-i\omega_4\tau}|^2. \end{aligned} \quad (5)$$

The coincidence probability $P_{40}(\tau)$ in the 4/0 detection scheme is

$$P_{40}(\tau) = \frac{1}{1024}\int_0^\infty d\omega_1 d\omega_2 d\omega_3 d\omega_4 |I_{40}(\tau)|^2, \quad (6)$$

with

$$\begin{aligned}|I_{40}(\tau)|^2 = |&(f_{13}f_{24} + f_{14}f_{23})e^{-i\omega_1\tau}e^{-i\omega_2\tau} \\ &+ (f_{31}f_{42} + f_{32}f_{41})e^{-i\omega_3\tau}e^{-i\omega_4\tau} \\ &+ (f_{12}f_{34} + f_{14}f_{32})e^{-i\omega_1\tau}e^{-i\omega_3\tau} \\ &+ (f_{12}f_{43} + f_{13}f_{42})e^{-i\omega_1\tau}e^{-i\omega_4\tau} \\ &+ (f_{21}f_{34} + f_{24}f_{31})e^{-i\omega_2\tau}e^{-i\omega_3\tau} \\ &+ (f_{21}f_{43} + f_{23}f_{41})e^{-i\omega_2\tau}e^{-i\omega_4\tau}|^2. \end{aligned} \quad (7)$$

It is interesting to compare the six items in $|I_{22}(\tau)|^2$, $|I_{31}(\tau)|^2$, and $|I_{40}(\tau)|^2$: the first and second terms in $|I_{22}(\tau)|^2$ are positive; the second, fourth, and sixth items in $|I_{31}(\tau)|^2$ are positive; and all six items in $|I_{40}(\tau)|^2$ are positive. As calculated in the Appendix, the sign of these terms results from the sign of the transmission and reflection terms after the beam splitter (BS) in Fig. 1. These equations can be further simplified by assuming the exchanging symmetry of $f(\omega_s,\omega_i) = f(\omega_i,\omega_s)$.

III. ANALYSIS

For a given JSA of $f(\omega_s,\omega_i)$, using the equations of $P_{22}(\tau)$, $P_{31}(\tau)$, and $P_{40}(\tau)$, it is possible to simulate the HOM-type interference patterns. Three kinds of JSAs are shown in Figs. 2(a1)–2(c1), with Fig. 2(a1) spectrally uncorrelated, Fig. 2(b1) positively correlated, and Fig. 2(c1) negatively correlated. Without the loss of generality, we set the center wavelength of the JSAs at 1584 nm and set the bandwidth (full width at half maximum) of the signal and idler photons at 2 nm. Although the shape of the three JSAs is different, the marginal distributions for the signal and idler photons are the same. In other words, from the viewpoint of single photons, all the signal and idler photons have the same spectral distribution in Figs. 2(a1)–2(c1).

Figures 2(a2)–2(c2) show the HOM-type interference patterns for 2/2 detection schemes. It is noteworthy that, for the uncorrelated state [Fig. 2(a1)] and negatively correlated state [Fig. 2(b1)], the coincidence probability changes in a nonmonotonic manner, when the time delay changes from 0 to 10 ps. In contrast, the positively correlated state [Fig. 2(c1)] shows a monotonic interference pattern. Figures 2(a3)–2(c3) show the HOM-type interference patterns for 3/1 detection

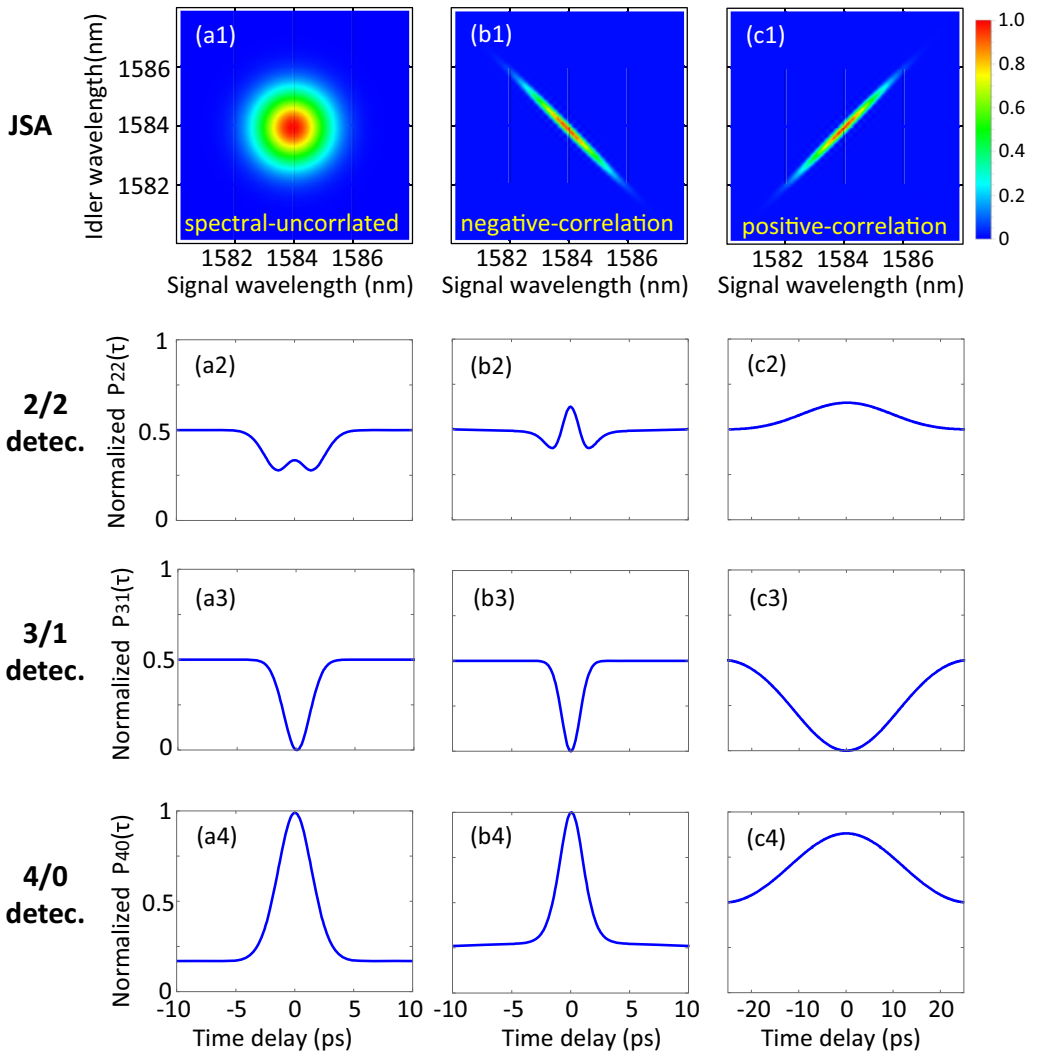

FIG. 2. Three different JSAs $f(\omega_s,\omega_i)$: (a1) uncorrelated, (b1) negatively correlated, and (c1) positively correlated. The corresponding HOM-type interference patterns are shown in (a2)–(c4): (a2)–(c2) 2/2 detection scheme, (a3)–(c3) 3/1 detection scheme, and (a4)–(c4) 4/0 detection scheme. All the y axes in (a2)–(c4) are normalized.

schemes, with all the figures in dips; i.e., the interference patterns are monotonic when the time delay changes from zero to infinity. The patterns for 4/0 detection are shown in Figs. 2(a4)–2(c4), with all the figures in bumps; i.e., the interference patterns show monotonic dependence.

In Fig. 2, biphotons with different correlations show different interference patterns, but what is the underlying physics for such phenomena? To answer this question, we need to further simplify Eqs. (3), (5), and (7). As an example, by assuming $f_{mn} = f_{nm}$, Eq. (3) can be simplified as follows:

$$
\begin{aligned}
|I_{22}(\tau)|^2 = {} & (f_{12}f_{34})^2 + (f_{13}f_{24})^2 + (f_{14}f_{23})^2 + f_{12}f_{13}f_{24}f_{34} + f_{12}f_{14}f_{23}f_{34} + f_{13}f_{14}f_{23}f_{24} \\
& + (f_{12}f_{34} + f_{13}f_{24})(f_{12}f_{34} + f_{14}f_{23})\cos(\omega_1 - \omega_2)\tau - (f_{12}f_{34} + f_{13}f_{24})(f_{13}f_{24} + f_{14}f_{23})\cos(\omega_1 - \omega_3)\tau \\
& - (f_{12}f_{34} + f_{14}f_{23})(f_{13}f_{24} + f_{14}f_{23})\cos(\omega_1 - \omega_4)\tau - (f_{12}f_{34} + f_{14}f_{23})(f_{13}f_{24} + f_{14}f_{23})\cos(\omega_2 - \omega_3)\tau \\
& - (f_{12}f_{34} + f_{13}f_{24})(f_{13}f_{24} + f_{14}f_{23})\cos(\omega_2 - \omega_4)\tau + (f_{12}f_{34} + f_{13}f_{24})(f_{12}f_{34} + f_{14}f_{23})\cos(\omega_3 - \omega_4)\tau \\
& + 1/2(f_{13}f_{24} + f_{14}f_{23})^2\cos(\omega_1 + \omega_2 - \omega_3 - \omega_4)\tau + 1/2(f_{12}f_{34} + f_{14}f_{23})^2\cos(\omega_1 - \omega_2 + \omega_3 - \omega_4)\tau \\
& + 1/2(f_{12}f_{34} + f_{13}f_{24})^2\cos(\omega_1 - \omega_2 - \omega_3 + \omega_4)\tau. \qquad (8)
\end{aligned}
$$

Obviously, Eq. (8) is a function of $\omega_m - \omega_n$. Similar results can also be derived for Eqs. (5) and (7). So, it can be concluded that *HOM-type multiphoton interference is a differential-frequency interference*. This is true not only for the two-photon HOM interference [14–16], but also for the four-photon HOM interference. Therefore, positively correlated biphotons, i.e.,

around $\omega_s - \omega_i = 0$, exhibit different patterns from that of the uncorrelated biphotons (ω_s and ω_i are arbitrary) or negatively correlated biphotons ($\omega_s + \omega_i = \omega_p$, with ω_p as the angular frequency of the pump).

The interference patterns in Figs. 2(c2)–2(c4) are "fatter" (the coherence time is longer) than the patterns in Figs. 2(a2)–2(a4) or Figs. 2(b2)–2(b4). It can also be explained from the above conclusion that HOM-type interference is a *differential-frequency* interference. In fact, Eq. (3) can be viewed as a Fourier transform from the frequency domain to the time domain. Consequently, the width of the time-domain interference pattern is determined by the spectral-domain distribution along the direction of $(\omega_s - \omega_i)$. The value of $(\omega_s - \omega_i)$ in Fig. 2(c1) is the smallest among Figs. 2(a1)–2(c1) in the frequency domain, so the corresponding widths in the interference patterns are the largest in the time domain, thanks to the spectral positive correlation in Fig. 2(c1).

It should be emphasized that the theoretical model of our scheme is different from the model in Refs. [1,12], where the spectral correlations are not included. The photons in the model of Refs. [1,12,17] are spectrally uncorrelated; therefore, the experimental results in Refs. [1,12] only correspond to Figs. 2(a2), 2(a3), and 2(a4) in our simulation.

Many studies have been dedicated to theoretically analyze multiphoton interference using multimode theory. Ou *et al.* analyzed multiphoton interference using multimode theory from spectral modes [2,10,18]; Chen *et al.* modeled the photons as wave packets in the time domain [19]; and Ra *et al.* considered Schmidt decomposition on the temporal modes of the photons in their theoretical model [1,12,13]. However, in all these theoretical models, the role of spectral correlation is not deeply investigated. Our model is a theoretical model for multiphoton interference with spectral correlation included.

It is interesting to compare the four-photon HOM interference with the case of the traditional two-photon HOM interference [7,20]. The twofold coincidence probability between two output ports of a beam splitter (antibunching test) can be written as

$$P_{11}(\tau) = \frac{1}{4}\int_0^\infty d\omega_1 d\omega_2 |I_{11}(\tau)|^2, \tag{9}$$

with

$$|I_{11}(\tau)|^2 = |f(\omega_2,\omega_1)e^{-i\omega_1\tau} - f(\omega_1,\omega_2)e^{-i\omega_2\tau}|^2. \tag{10}$$

In contrast, the twofold coincidence probability of one output port of the beam splitter (bunching test) can be written as

$$P_{20}(\tau) = \frac{1}{16}\int_0^\infty d\omega_1 d\omega_2 |I_{20}(\tau)|^2, \tag{11}$$

with

$$|I_{20}(\tau)|^2 = |f(\omega_2,\omega_1)e^{-i\omega_1\tau} + f(\omega_1,\omega_2)e^{-i\omega_2\tau}|^2. \tag{12}$$

We also simulated $P_{11}(\tau)$ and $P_{20}(\tau)$ using the three JSAs shown in Figs. 2(a1)–2(c1). It was found that the monotonicity was not affected by the spectral correlations; i.e., all three $P_{11}(\tau)$ patterns show dips, while all three $P_{20}(\tau)$ patterns show bumps for the JSAs in Figs. 2(a1)–2(c1).

It is also important to rethink the prerequisite condition for 100% visibility in the two-photon and four-photon HOM interference. In the two-photon case, *exchanging symmetry* of $f(\omega_1,\omega_2) = f(\omega_2,\omega_1)$ is required to achieve 100% visibility, i.e., $P_{11}(0) = 0$ [20,21]. In contrast, the prerequisite condition is complex for the four-photon HOM interference to achieve 100% visibility. For example, in the case of 3/1 detection, $P_{31}(0) = 0$ implies $-(f_{13}f_{24} + f_{14}f_{23}) + (f_{31}f_{42} + f_{32}f_{41}) - (f_{12}f_{34} + f_{14}f_{32}) + (f_{12}f_{43} + f_{13}f_{42}) - (f_{21}f_{34} + f_{24}f_{31}) + (f_{21}f_{43} + f_{23}f_{41}) = 0$, which is an upgraded version of the *exchanging symmetry* for the four-photon case.

In the theoretical model in Eq. (1), the four-photon state is generated from a double pair emission, which has a spectral distribution of $f(\omega_s,\omega_i)f(\omega_s',\omega_i')$. In the future, it will be possible to directly generate a four-photon state with a spectral distribution of $f(\omega_s,\omega_i,\omega_s',\omega_i')$. This state may be generated from, say, a fourth-order spontaneous parametric down-conversion process, where a higher-energy photon "splits" into four lower-energy photons. For example, a 1600-nm photon may be down-converted to four 400-nm photons. This is the inverse process of a fourth-harmonic generation. The direct generation of the three-photon state has been chased by several groups for a long time [22–25]. It is also interesting to study the case of the four-photon state [26–28]. In this case, the spectral correlations and the HOM interference might be different from the case discussed in this paper. It will be an interesting topic to investigate in the future. Another future work is to expand the theoretical model to the case of six or more photons. Although the equations might be complex, the expansion method is direct, i.e., similar to what we did in this work.

For the future experimental demonstration, our scheme has been ready to be realized with state-of-the-art technologies. The spectrally uncorrelated JSA in Fig. 2(a1) can be generated by filtering a periodically poled potassium titanyl phosphate (PPKTP) down-conversion source at 1584 nm [29–31]. The spectrally negatively correlated JSA in Fig. 2(b1) has been generated in a picosecond-pulse-pumped periodically poled stoichiometric lithium tantalate (PPSLT) crystal [21], while the spectrally positively correlated JSA in Fig. 2(c1) has been prepared in a femtosecond-pulse-pumped PPKTP crystal [21]. For detection, we can use the similar setup demonstrated recently [32].

Our work has several applications in the future. Higher-order correlations in many-body systems are very important for characterizing a quantum system and came to be a hot topic in the study of quantum optics [17,33,34]. In this work, we studied the role of spectral correlation in four-photon quantum interference, which actually corresponds to a fourth-order temporal correlation in a four-body system. Therefore, this work may make a contribution to the deep understanding of higher-order correlations of a quantum system. Another possible application of our work is for quantum sensing based on Hong-Ou-Mandel interference [35–37]. Third, the spectral correlation may be applied to the reduction of detection noise in a dispersive medium, which was recently demonstrate in Ref. [38] with only two photons. In the case of four photons, the noise-reduction effect might be enhanced.

IV. CONCLUSION

In conclusion, we have investigated the role of spectral correlation (frequency entanglement) in quantum-to-classical transition in a four-photon Hong-Ou-Mandel interference. By

theoretical calculation and numerical simulation based on a multimode theory for spectrally correlated photons, it was found that the transition can be monotonic for positively correlated biphotons and can be nonmonotonic for negatively correlated or noncorrelated biphotons in the 2/2 detection scheme. In contrast, the monotonicity was not changed in the 3/1 and 4/0 detection schemes. The fundamental reason for this difference is that the HOM-type interference is a differential-frequency interference. Our theoretical scheme can be easily demonstrated in experiment using the state-of-the-art technologies. This study may shed new light on understanding the role of entanglement in multiphoton behavior.

ACKNOWLEDGMENTS

The authors are grateful to M. Takeoka for helpful discussions. R.-B.J. is supported by the Fund from the Educational Department of Hubei Province, China (Grant No. D20161504). C.L.R. is supported by the Youth Innovation Promotion Association (CAS) Grant No. 2015317, National Natural Science Foundations of China (Grant No. 11605205), and Natural Science Foundations of Chong Qing (Grant No. cstc2015jcyjA00021). H.J. is supported by the National Natural Science Foundations of China (Grant No. 11474087).

APPENDIX

Here we deduce the equations for the four-photon HOM-type interference in detail. The setup of HOM interference with 2/2 detection scheme is shown in Fig. 1(a). The two-pair component from a SPDC process is expressed as [Eq. (1) in the main text]

$$|\psi\rangle = \int_0^\infty d\omega_s d\omega_i d\omega_s' d\omega_i' f(\omega_s,\omega_i) f(\omega_s',\omega_i') \hat{a}_s^\dagger(\omega_s)\hat{a}_i^\dagger(\omega_i)\hat{a}_s^\dagger(\omega_s')\hat{a}_i^\dagger(\omega_i')|0000\rangle. \tag{A1}$$

The meaning of each parameter is explained in the main text. The detection field operator of detector D_n ($n = 1,2,3,4$) is

$$\hat{E}_n^{(+)}(t_n) = \frac{1}{\sqrt{2\pi}} \int_0^\infty d\omega_n \hat{a}_n(\omega_n) e^{-i\omega_n t_n}, \tag{A2}$$

where ω_n is the frequency of the detection field, and $\hat{a}_n$ is the annihilation operator of the detection field. The transformation rule of a 50:50 beam splitter is $\hat{a}_{o_1} = \frac{1}{\sqrt{2}}(\hat{a}_{in_1} + \hat{a}_{in_2})$ and $\hat{a}_{o_2} = \frac{1}{\sqrt{2}}(\hat{a}_{in_1} - \hat{a}_{in_2})$, where the subscripts o_1 and o_2 denote the two output ports of the beam splitter, while the in_1 and in_2 denote the two input ports.

So, we can write the detection fields as

$$\begin{aligned}
\hat{E}_1^{(+)}(t_1) &= \frac{1}{2\sqrt{2\pi}} \int_0^\infty d\omega_1 [\hat{a}_s(\omega_1) e^{-i\omega_1\tau} + \hat{a}_i(\omega_1)] e^{-i\omega_1 t_1}, \\
\hat{E}_2^{(+)}(t_2) &= \frac{1}{2\sqrt{2\pi}} \int_0^\infty d\omega_2 [\hat{a}_s(\omega_2) e^{-i\omega_2\tau} + \hat{a}_i(\omega_2)] e^{-i\omega_2 t_2}, \\
\hat{E}_3^{(+)}(t_3) &= \frac{1}{2\sqrt{2\pi}} \int_0^\infty d\omega_3 [\hat{a}_s(\omega_3) e^{-i\omega_3\tau} - \hat{a}_i(\omega_3)] e^{-i\omega_3 t_3}, \\
\hat{E}_4^{(+)}(t_4) &= \frac{1}{2\sqrt{2\pi}} \int_0^\infty d\omega_4 [\hat{a}_s(\omega_4) e^{-i\omega_4\tau} - \hat{a}_i(\omega_4)] e^{-i\omega_4 t_4},
\end{aligned} \tag{A3}$$

where the phase term $e^{-i\omega_n\tau}$ is introduced by the time delay τ. The coincidence probability P_{22} as a function of delay time τ can be expressed as

$$P_{22}(\tau) = \int dt_1 dt_2 dt_3 dt_4 \langle\psi|\hat{E}_4^{(-)}\hat{E}_3^{(-)}\hat{E}_2^{(-)}\hat{E}_1^{(-)}\hat{E}_1^{(+)}\hat{E}_2^{(+)}\hat{E}_3^{(+)}\hat{E}_4^{(+)}|\psi\rangle. \tag{A4}$$

First, let us consider the $\hat{E}_1^{(+)}\hat{E}_2^{(+)}\hat{E}_3^{(+)}\hat{E}_4^{(+)}|\psi\rangle$. For simplicity, the key components can be written as $[\hat{a}_s(\omega_1) + \hat{a}_i(\omega_1)][\hat{a}_s(\omega_2) + \hat{a}_i(\omega_2)][\hat{a}_s(\omega_3) - \hat{a}_i(\omega_3)][\hat{a}_s(\omega_4) - \hat{a}_i(\omega_4)]$. Only 6 out of 16 terms exist: $\hat{a}_s\hat{a}_s\hat{a}_i\hat{a}_i$, $\hat{a}_i\hat{a}_i\hat{a}_s\hat{a}_s$, $-\hat{a}_s\hat{a}_i\hat{a}_s\hat{a}_i$, $-\hat{a}_s\hat{a}_i\hat{a}_i\hat{a}_s$, $-\hat{a}_i\hat{a}_s\hat{a}_s\hat{a}_i$, and $-\hat{a}_i\hat{a}_s\hat{a}_i\hat{a}_s$. The first term $(\hat{a}_s\hat{a}_s\hat{a}_i\hat{a}_i)$ is

$$\begin{aligned}
&\frac{1}{16}\left(\frac{1}{2\pi}\right)^2 \int_0^\infty d\omega_1 d\omega_2 d\omega_3 d\omega_4 \hat{a}_s(\omega_1)\hat{a}_s(\omega_2)\hat{a}_i(\omega_3)\hat{a}_i(\omega_4) e^{-i\omega_1\tau} e^{-i\omega_2\tau} e^{-i\omega_1 t_1} e^{-i\omega_2 t_2} e^{-i\omega_3 t_3} e^{-i\omega_4 t_4} \\
&\quad \times \int_0^\infty d\omega_s d\omega_i d\omega_{s'} d\omega_{i'} f(\omega_s,\omega_i) f(\omega_s',\omega_i') \hat{a}_s^\dagger(\omega_s)\hat{a}_i^\dagger(\omega_i)\hat{a}_s^\dagger(\omega_s')\hat{a}_i^\dagger(\omega_i')|0\rangle \\
&= \frac{1}{16}\left(\frac{1}{2\pi}\right)^2 \int_0^\infty d\omega_1 d\omega_2 d\omega_3 d\omega_4 \int_0^\infty d\omega_s d\omega_i d\omega_{s'} d\omega_{i'} [\delta(\omega_1 - \omega_s)\delta(\omega_2 - \omega_{s'}) + \delta(\omega_1 - \omega_{s'})\delta(\omega_2 - \omega_s)][\delta(\omega_3 - \omega_i) \\
&\quad \times \delta(\omega_4 - \omega_{i'}) + \delta(\omega_3 - \omega_{i'})\delta(\omega_4 - \omega_i)] f(\omega_s,\omega_i) f(\omega_s',\omega_i') e^{-i\omega_1\tau} e^{-i\omega_2\tau} e^{-i\omega_1 t_1} e^{-i\omega_2 t_2} e^{-i\omega_3 t_3} e^{-i\omega_4 t_4}|0\rangle \\
&= \frac{1}{16}\left(\frac{1}{2\pi}\right)^2 \int_0^\infty d\omega_1 d\omega_2 d\omega_3 d\omega_4 [f(\omega_1,\omega_3) f(\omega_2,\omega_4) + f(\omega_1,\omega_4) f(\omega_2,\omega_3) + f(\omega_2,\omega_3) f(\omega_1,\omega_4)
\end{aligned}$$

$$+ f(\omega_2,\omega_4)f(\omega_1,\omega_3)]e^{-i\omega_1\tau}e^{-i\omega_2\tau}e^{-i\omega_1 t_1}e^{-i\omega_2 t_2}e^{-i\omega_3 t_3}e^{-i\omega_4 t_4}|0\rangle$$
$$= \frac{1}{8}\left(\frac{1}{2\pi}\right)^2\int_0^\infty d\omega_1 d\omega_2 d\omega_3 d\omega_4[f(\omega_1,\omega_3)f(\omega_2,\omega_4)+f(\omega_1,\omega_4)f(\omega_2,\omega_3)]e^{-i\omega_1\tau}e^{-i\omega_2\tau}e^{-i\omega_1 t_1}e^{-i\omega_2 t_2}e^{-i\omega_3 t_3}e^{-i\omega_4 t_4}|0\rangle$$
$$= \frac{1}{8}\left(\frac{1}{2\pi}\right)^2\int_0^\infty d\omega_1 d\omega_2 d\omega_3 d\omega_4 \times ff_1 \times e^{-i\omega_1 t_1}e^{-i\omega_2 t_2}e^{-i\omega_3 t_3}e^{-i\omega_4 t_4}|0\rangle, \tag{A5}$$

where

$$ff_1 = [f(\omega_1,\omega_3)f(\omega_2,\omega_4)+f(\omega_1,\omega_4)f(\omega_2,\omega_3)]e^{-i\omega_1\tau}e^{-i\omega_2\tau}. \tag{A6}$$

In the above calculation, the following relationship is used:

$$\hat{a}_s(\omega_1)\hat{a}_s(\omega_2)\hat{a}_s^\dagger(\omega_s)\hat{a}_s^\dagger(\omega_s')|0\rangle = [\delta(\omega_1-\omega_s)\delta(\omega_2-\omega_{s'})+\delta(\omega_1-\omega_{s'})\delta(\omega_2-\omega_s)]|0\rangle. \tag{A7}$$

Similarly, the second term ($\hat{a}_i\hat{a}_i\hat{a}_s\hat{a}_s$) is

$$\frac{1}{8}\left(\frac{1}{2\pi}\right)^2\int_0^\infty d\omega_1 d\omega_2 d\omega_3 d\omega_4 \times ff_2 \times e^{-i\omega_1 t_1}e^{-i\omega_2 t_2}e^{-i\omega_3 t_3}e^{-i\omega_4 t_4}|0\rangle, \tag{A8}$$

where

$$ff_2 = [f(\omega_3,\omega_1)f(\omega_4,\omega_2,)+f(\omega_3,\omega_2)f(\omega_4,\omega_1)]e^{-i\omega_3\tau}e^{-i\omega_4\tau}. \tag{A9}$$

The third term ($-\hat{a}_s\hat{a}_i\hat{a}_s\hat{a}_i$) is

$$\frac{1}{8}\left(\frac{1}{2\pi}\right)^2\int_0^\infty d\omega_1 d\omega_2 d\omega_3 d\omega_4 \times ff_3 \times e^{-i\omega_1 t_1}e^{-i\omega_2 t_2}e^{-i\omega_3 t_3}e^{-i\omega_4 t_4}|0\rangle, \tag{A10}$$

where

$$ff_3 = [-f(\omega_1,\omega_2)f(\omega_3,\omega_4)-f(\omega_1,\omega_4)f(\omega_3,\omega_2)]e^{-i\omega_1\tau}e^{-i\omega_3\tau}. \tag{A11}$$

The fourth term ($-\hat{a}_s\hat{a}_i\hat{a}_i\hat{a}_s$) is

$$\frac{1}{8}\left(\frac{1}{2\pi}\right)^2\int_0^\infty d\omega_1 d\omega_2 d\omega_3 d\omega_4 \times ff_4 \times e^{-i\omega_1 t_1}e^{-i\omega_2 t_2}e^{-i\omega_3 t_3}e^{-i\omega_4 t_4}|0\rangle, \tag{A12}$$

where

$$ff_4 = [-f(\omega_1,\omega_2)f(\omega_4,\omega_3)-f(\omega_1,\omega_3)f(\omega_4,\omega_2)]e^{-i\omega_1\tau}e^{-i\omega_4\tau}. \tag{A13}$$

The fifth term ($-\hat{a}_i\hat{a}_s\hat{a}_s\hat{a}_i$) is

$$\frac{1}{8}\left(\frac{1}{2\pi}\right)^2\int_0^\infty d\omega_1 d\omega_2 d\omega_3 d\omega_4 \times ff_5 \times e^{-i\omega_1 t_1}e^{-i\omega_2 t_2}e^{-i\omega_3 t_3}e^{-i\omega_4 t_4}|0\rangle, \tag{A14}$$

where

$$ff_5 = [-f(\omega_2,\omega_1)f(\omega_3,\omega_4)-f(\omega_2,\omega_4)f(\omega_3,\omega_1)]e^{-i\omega_2\tau}e^{-i\omega_3\tau}. \tag{A15}$$

The sixth term ($-\hat{a}_i\hat{a}_s\hat{a}_i\hat{a}_s$) is

$$\frac{1}{8}\left(\frac{1}{2\pi}\right)^2\int_0^\infty d\omega_1 d\omega_2 d\omega_3 d\omega_4 \times ff_6 \times e^{-i\omega_1 t_1}e^{-i\omega_2 t_2}e^{-i\omega_3 t_3}e^{-i\omega_4 t_4}|0\rangle, \tag{A16}$$

where

$$ff_6 = [-f(\omega_2,\omega_1)f(\omega_4,\omega_3)-f(\omega_2,\omega_3)f(\omega_4,\omega_1)]e^{-i\omega_2\tau}e^{-i\omega_4\tau}. \tag{A17}$$

We combine these six terms:

$$\hat{E}_1^{(+)}\hat{E}_2^{(+)}\hat{E}_3^{(+)}\hat{E}_4^{(+)}|\psi\rangle = \frac{1}{8}\left(\frac{1}{2\pi}\right)^2\int_0^\infty d\omega_1 d\omega_2 d\omega_3 d\omega_4(ff_1+ff_2+ff_3+ff_4+ff_5+ff_6)e^{-i\omega_1 t_1}e^{-i\omega_2 t_2}e^{-i\omega_3 t_3}e^{-i\omega_4 t_4}|0\rangle. \tag{A18}$$

Then

$$\langle\psi|\hat{E}_4^{(-)}\hat{E}_3^{(-)}\hat{E}_2^{(-)}\hat{E}_1^{(-)}\hat{E}_1^{(+)}\hat{E}_2^{(+)}\hat{E}_3^{(+)}\hat{E}_4^{(+)}|\psi\rangle$$
$$= \frac{1}{8}\left(\frac{1}{2\pi}\right)^2\int_0^\infty d\omega_1 d\omega_2 d\omega_3 d\omega_4(ff_1+ff_2+ff_3+ff_4+ff_5+ff_6)e^{-i\omega_1 t_1}e^{-i\omega_2 t_2}e^{-i\omega_3 t_3}e^{-i\omega_4 t_4}\frac{1}{8}\left(\frac{1}{2\pi}\right)^2$$
$$\times\int_0^\infty d\omega_1' d\omega_2' d\omega_3' d\omega_4'(ff_1^*+ff_2^*+ff_3^*+ff_4^*+ff_5^*+ff_6^*)e^{i\omega_1' t_1}e^{i\omega_2' t_2}e^{i\omega_3' t_3}e^{i\omega_4' t_4}, \tag{A19}$$

where ff^* is the complex conjugate of ff.

Finally,

$$\begin{aligned}
P_{22}(\tau) &= \int dt_1 dt_2 dt_3 dt_4 \langle\psi|\hat{E}_4^{(-)}\hat{E}_3^{(-)}\hat{E}_2^{(-)}\hat{E}_1^{(-)}\hat{E}_1^{(+)}\hat{E}_2^{(+)}\hat{E}_3^{(+)}\hat{E}_4^{(+)}|\psi\rangle \\
&= \frac{1}{64}\left(\frac{1}{2\pi}\right)^4 \int dt_1 dt_2 dt_3 dt_4 \int_0^\infty d\omega_1 d\omega_2 d\omega_3 d\omega_4 \int_0^\infty d\omega_1' d\omega_2' d\omega_3' d\omega_4' (ff_1 + ff_2 + ff_3 + ff_4 + ff_5 + ff_6) \\
&\quad \times (ff_1^* + ff_2^* + ff_3^* + ff_4^* + ff_5^* + ff_6^*) e^{-i\omega_1 t_1} e^{-i\omega_2 t_2} e^{-i\omega_3 t_3} e^{-i\omega_4 t_4} e^{i\omega_1' t_1} e^{i\omega_2' t_2} e^{i\omega_3' t_3} e^{i\omega_4' t_4} \\
&= \frac{1}{64}\left(\frac{1}{2\pi}\right)^4 \int_0^\infty d\omega_1 d\omega_2 d\omega_3 d\omega_4 \int_0^\infty d\omega_1' d\omega_2' d\omega_3' d\omega_4' (ff_1 + ff_2 + ff_3 + ff_4 + ff_5 + ff_6) \\
&\quad \times (ff_1^* + ff_2^* + ff_3^* + ff_4^* + ff_5^* + ff_6^*) (2\pi)^4 \delta(\omega_1 - \omega_1') \delta(\omega_2 - \omega_2') \delta(\omega_3 - \omega_3') \delta(\omega_4 - \omega_4') \\
&= \frac{1}{64} \int_0^\infty d\omega_1 d\omega_2 d\omega_3 d\omega_4 |ff_1 + ff_2 + ff_3 + ff_4 + ff_5 + ff_6|^2. \qquad \text{(A20)}
\end{aligned}$$

In the above calculation, the relationship of $\delta(\omega - \omega') = \frac{1}{2\pi}\int_{-\infty}^{\infty} e^{i(\omega-\omega')t} dt$ is used.

In conclusion, the fourfold coincidence probability in the 2/2 detection scheme is

$$P_{22}(\tau) = \frac{1}{64} \int_0^\infty d\omega_1 d\omega_2 d\omega_3 d\omega_4 |I_{22}(\tau)|^2, \qquad \text{(A21)}$$

with

$$\begin{aligned}
|I_{22}(\tau)|^2 &= |(f_{13}f_{24} + f_{14}f_{23}) e^{-i\omega_1\tau} e^{-i\omega_2\tau} + (f_{31}f_{42} + f_{32}f_{41}) e^{-i\omega_3\tau} e^{-i\omega_4\tau} - (f_{12}f_{34} + f_{14}f_{32}) e^{-i\omega_1\tau} e^{-i\omega_3\tau} \\
&\quad - (f_{12}f_{43} + f_{13}f_{42}) e^{-i\omega_1\tau} e^{-i\omega_4\tau} - (f_{21}f_{34} + f_{24}f_{31}) e^{-i\omega_2\tau} e^{-i\omega_3\tau} - (f_{21}f_{43} + f_{23}f_{41}) e^{-i\omega_2\tau} e^{-i\omega_4\tau}|^2, \qquad \text{(A22)}
\end{aligned}$$

where $f_{ij} = f(\omega_i, \omega_j)$.

In the 3/1 detection, the key components can be written as $[\hat{a}_s(\omega_1) + \hat{a}_i(\omega_1)][\hat{a}_s(\omega_2) + \hat{a}_i(\omega_2)][\hat{a}_s(\omega_3) + \hat{a}_i(\omega_3)][\hat{a}_s(\omega_4) - \hat{a}_i(\omega_4)]$. Only 6 out of 16 terms exist: $-\hat{a}_s\hat{a}_s\hat{a}_i\hat{a}_i$, $\hat{a}_i\hat{a}_i\hat{a}_s\hat{a}_s$, $-\hat{a}_s\hat{a}_i\hat{a}_s\hat{a}_i$, $\hat{a}_s\hat{a}_i\hat{a}_i\hat{a}_s$, $-\hat{a}_i\hat{a}_s\hat{a}_s\hat{a}_i$, and $\hat{a}_i\hat{a}_s\hat{a}_i\hat{a}_s$. Following the similar method as in the case of 2/2 detection, the coincidence probability $P_{31}(\tau)$ in the 3/1 detection scheme can be calculated as

$$P_{31}(\tau) = \frac{1}{128} \int_0^\infty d\omega_1 d\omega_2 d\omega_3 d\omega_4 |I_{31}(\tau)|^2, \qquad \text{(A23)}$$

with

$$\begin{aligned}
|I_{31}(\tau)|^2 &= |-(f_{13}f_{24} + f_{14}f_{23}) e^{-i\omega_1\tau} e^{-i\omega_2\tau} + (f_{31}f_{42} + f_{32}f_{41}) e^{-i\omega_3\tau} e^{-i\omega_4\tau} - (f_{12}f_{34} + f_{14}f_{32}) e^{-i\omega_1\tau} e^{-i\omega_3\tau} \\
&\quad + (f_{12}f_{43} + f_{13}f_{42}) e^{-i\omega_1\tau} e^{-i\omega_4\tau} - (f_{21}f_{34} + f_{24}f_{31}) e^{-i\omega_2\tau} e^{-i\omega_3\tau} + (f_{21}f_{43} + f_{23}f_{41}) e^{-i\omega_2\tau} e^{-i\omega_4\tau}|^2. \qquad \text{(A24)}
\end{aligned}$$

In the 4/0 detection, the key components can be written as $[\hat{a}_s(\omega_1) + \hat{a}_i(\omega_1)][\hat{a}_s(\omega_2) + \hat{a}_i(\omega_2)][\hat{a}_s(\omega_3) + \hat{a}_i(\omega_3)][\hat{a}_s(\omega_4) + \hat{a}_i(\omega_4)]$. Only 6 out of 16 terms exist: $\hat{a}_s\hat{a}_s\hat{a}_i\hat{a}_i$, $\hat{a}_i\hat{a}_i\hat{a}_s\hat{a}_s$, $\hat{a}_s\hat{a}_i\hat{a}_s\hat{a}_i$, $\hat{a}_s\hat{a}_i\hat{a}_i\hat{a}_s$, $\hat{a}_i\hat{a}_s\hat{a}_s\hat{a}_i$, and $\hat{a}_i\hat{a}_s\hat{a}_i\hat{a}_s$. The coincidence probability $P_{40}(\tau)$ in the 4/0 detection scheme is

$$P_{40}(\tau) = \frac{1}{1024} \int_0^\infty d\omega_1 d\omega_2 d\omega_3 d\omega_4 |I_{40}(\tau)|^2, \qquad \text{(A25)}$$

with

$$\begin{aligned}
|I_{40}(\tau)|^2 &= |(f_{13}f_{24} + f_{14}f_{23}) e^{-i\omega_1\tau} e^{-i\omega_2\tau} + (f_{31}f_{42} + f_{32}f_{41}) e^{-i\omega_3\tau} e^{-i\omega_4\tau} + (f_{12}f_{34} + f_{14}f_{32}) e^{-i\omega_1\tau} e^{-i\omega_3\tau} \\
&\quad + (f_{12}f_{43} + f_{13}f_{42}) e^{-i\omega_1\tau} e^{-i\omega_4\tau} + (f_{21}f_{34} + f_{24}f_{31}) e^{-i\omega_2\tau} e^{-i\omega_3\tau} + (f_{21}f_{43} + f_{23}f_{41}) e^{-i\omega_2\tau} e^{-i\omega_4\tau}|^2. \qquad \text{(A26)}
\end{aligned}$$

[1] Y.-S. Ra, M. C. Tichy, H.-T. Lim, O. Kwon, F. Mintert, A. Buchleitner, and Y.-H. Kim, Proc. Natl. Acad. Sci. USA **110**, 1227 (2013).

[2] Z.-Y. J. Ou, *Multi-photon Quantum Interference* (Springer, New York, 2007).

[3] P. J. Mosley, J. S. Lundeen, B. J. Smith, P. Wasylczyk, A. B. U'Ren, C. Silberhorn, and I. A. Walmsley, Phys. Rev. Lett. **100**, 133601 (2008).

[4] P. J. Mosley, J. S. Lundeen, B. J. Smith, and I. A. Walmsley, New J. Phys. **10**, 093011 (2008).

[5] R.-B. Jin, K. Wakui, R. Shimizu, H. Benichi, S. Miki, T. Yamashita, H. Terai, Z. Wang, M. Fujiwara, and M. Sasaki, Phys. Rev. A **87**, 063801 (2013).

[6] R.-B. Jin, J. Zhang, R. Shimizu, N. Matsuda, Y. Mitsumori, H. Kosaka, and K. Edamatsu, Phys. Rev. A **83**, 031805 (2011).

[7] C. K. Hong, Z. Y. Ou, and L. Mandel, Phys. Rev. Lett. **59**, 2044 (1987).
[8] M. Arndt, A. Buchleitner, R. N. Mantegna, and H. Walther, Phys. Rev. Lett. **67**, 2435 (1991).
[9] D. A. Steck, V. Milner, W. H. Oskay, and M. G. Raizen, Phys. Rev. E **62**, 3461 (2000).
[10] Z. Y. Ou, J.-K. Rhee, and L. J. Wang, Phys. Rev. Lett. **83**, 959 (1999).
[11] X.-L. Niu, Y.-X. Gong, B.-H. Liu, Y.-F. Huang, G.-C. Guo, and Z. Y. Ou, Opt. Lett. **34**, 1297 (2009).
[12] Y.-S. Ra, M. C. Tichy, H.-T. Lim, O. Kwon, F. Mintert, A. Buchleitner, and Y.-H. Kim, Nat. Commun. **4**, 2451 (2013).
[13] M. C. Tichy, H.-T. Lim, Y.-S. Ra, F. Mintert, Y.-H. Kim, and A. Buchleitner, Phys. Rev. A **83**, 062111 (2011).
[14] V. Giovannetti, L. Maccone, J. H. Shapiro, and F. N. C. Wong, Phys. Rev. Lett. **88**, 183602 (2002).
[15] K. Wang, J. Phys. B: At. Mol. Opt. Phys. **39**, R293 (2006).
[16] R.-B. Jin, R. Shimizu, M. Fujiwara, M. Takeoka, R. Wakabayashi, T. Yamashita, S. Miki, H. Terai, T. Gerrits, and M. Sasaki, Quantum Sci. Technol. **1**, 015004 (2016).
[17] Y.-S. Ra, M. C. Tichy, H.-T. Lim, C. Gneiting, K. Molmer, A. Buchleitner, and Y.-H. Kim, arXiv:1703.01140.
[18] Z. Y. Ou, J.-K. Rhee, and L. J. Wang, Phys. Rev. A **60**, 593 (1999).
[19] L. Chen, C.-F. Li, M. Gong, F.-W. Sun, and G.-C. Guo, Europhys. Lett. **85**, 14001 (2009).
[20] R.-B. Jin, T. Gerrits, M. Fujiwara, R. Wakabayashi, T. Yamashita, S. Miki, H. Terai, R. Shimizu, M. Takeoka, and M. Sasaki, Opt. Express **23**, 28836 (2015).
[21] R. Shimizu and K. Edamatsu, Opt. Express **17**, 16385 (2009).
[22] D. Bouwmeester, J.-W. Pan, M. Daniell, H. Weinfurter, and A. Zeilinger, Phys. Rev. Lett. **82**, 1345 (1999).
[23] C. Ren and H. F. Hofmann, Phys. Rev. A **86**, 014301 (2012).
[24] L. K. Shalm, D. R. Hamel, Z. Yan, C. Simon, K. J. Resch, and T. Jennewein, Nat. Phys. **9**, 19 (2013).
[25] S. Agne, T. Kauten, J. Jin, E. Meyer-Scott, J. Z. Salvail, D. R. Hamel, K. J. Resch, G. Weihs, and T. Jennewein, Phys. Rev. Lett. **118**, 153602 (2017).
[26] H. D. Riedmatten, V. Scarani, I. Marcikic, A. Acín, W. Tittel, H. Zbinden, and N. Gisin, J. Mod. Opt. **51**, 1637 (2004).
[27] M. Wang and F. Yan, Int. J. Quantum Inf. **13**, 1550024 (2015).
[28] B. C. Hiesmayr, M. J. A. de Dood, and W. Loffler, Phys. Rev. Lett. **116**, 073601 (2016).
[29] R.-B. Jin, R. Shimizu, K. Wakui, H. Benichi, and M. Sasaki, Opt. Express **21**, 10659 (2013).
[30] N. Bruno, A. Martin, T. Guerreiro, B. Sanguinetti, and R. T. Thew, Opt. Express **22**, 17246 (2014).
[31] R.-B. Jin, P. Zhao, P. Deng, and Q.-L. Wu, Phys. Rev. Appl. **6**, 064017 (2016).
[32] R.-B. Jin, M. Fujiwara, R. Shimizu, R. J. Collins, G. S. Buller, T. Yamashita, S. Miki, H. Terai, M. Takeoka, and M. Sasaki, Sci. Rep. **6**, 36914 (2016).
[33] T. Schweigler, V. Kasper, S. Erne, I. Mazets, B. Rauer, F. Cataldini, T. Langen, T. Gasenzer, J. Berges, and J. Schmiedmayer, Nature (London) **545**, 323 (2017).
[34] M. C. Tichy, J. Phys. B: At. Mol. Opt. Phys. **47**, 103001 (2014).
[35] S. Basiri-Esfahani, C. R. Myers, A. Armin, J. Combes, and G. J. Milburn, Opt. Express **23**, 16008 (2015).
[36] M. Hou, Y. Wang, S. Liu, J. Guo, Z. Li, and P. Lu, J. Lightw. Technol. **32**, 4035 (2014).
[37] S. Liu, Z. Wang, M. Hou, J. Tian, and J. Xia, Opt. Laser Technol. **82**, 53 (2016).
[38] K. Sedziak, M. Lasota, and P. Kolenderski, Optica **4**, 84 (2017).